Additive Manufacturing 75 (2023) 103752

Contents lists available at ScienceDirect

Additive Manufacturing

journal homepage: www.elsevier.com/locate/addma

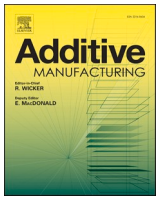

Printing by yield stress fluid shaping

A. Geffrault [a,b], H. Bessaies-Bey [b], N. Roussel [b], P. Coussot [a,*]

[a] Lab. Navier, Ecole des Ponts, Univ Gustave Eiffel, CNRS, 77420 Marne la Vallée, France
[b] MAST-CPDM, Univ Gustave Eiffel, 77420 Marne la Vallée, France

ARTICLE INFO

Keywords:
Yield stress fluid
Filament
Drop
Meandering
Loops
Classification

ABSTRACT

3D printing of yield stress fluids (i.e., materials able to flow like liquids only beyond a critical stress) is opening new doors in the fields of construction, food or medicine. The usual printing technique consists to extrude and then deposit a filament of yield stress fluid onto the previous layer. One major difficulty is that, during the deposition process, some instabilities may appear and have a catastrophic impact on the final 3D structure. Here we show that these instabilities can be predicted as a function of the material properties and/or the printing parameters. More generally, we study the deposit of a filament from systematic tests with a model yield stress fluid, varying the material yield stress value, the distance between the nozzle and the substrate, the extrusion velocity, the nozzle diameter, and the nozzle displacement velocity. We show that a diversity of patterns arises: drops, discontinuous lines, straight lines, meanders, alternated loops or translated loops. Then, we demonstrate that the transitions (frontier curves) between pattern regions can be predicted by theoretical arguments. Finally, we present a generic diagram predicting the patterns observed as a function of dimensionless numbers depending on the various characteristics of the system. This provides a reference scheme for optimizing practical processes or devising specific deposit patterns, valid for a wide range of conditions and yield stress fluids.

1. Introduction

Standard additive manufacturing generally involves the deposition of successive layers of a liquid initially of low viscosity which may rapidly solidify thanks to some temperature decrease or chemical reaction, so that it can withstand the next layer. Such additive manufacturing technology has now been applied for decades to viscoelastic solutions of polymers. There is also a wide range of materials, such as foams, concentrated emulsions, dense mineral suspensions, physical gels, which may all, in principle, be shaped through some additive manufacturing process. The common specificity of these materials at the origin of their ability to be printed is that they are yield stress fluids, i.e., they behave as solids below a critical stress (i.e., the yield stress, here noted τ_c) associated with a critical deformation, and behave as liquids beyond this stress or deformation. In the latter state, they can be deformed at will but keep their mechanical properties, which explains that we globally consider them as fluids [1]. In the last two decades, yield stress fluid printing developed in various fields such as construction materials (cement, concrete, raw earth) [2–7], electronics [8], energy devices [9], ceramics [10], food industry [11,12], medicine [13]. Note that embedded 3D printing also develops, in which an initially simple liquid is injected through a yield stress fluid which tends to fix its shape [14–17], but this is out of the scope of the present study.

This rheological behavior has a significant impact on the printing conditions if the yield stress is significant with regards to gravity and capillary effects, i.e. when τ_c is in the same order as or larger than the characteristic gravity stress ρgh, in which ρ is the material density, g the gravity and h a characteristic thickness of the material in the process [18], or if τ_c is in the same order as or larger than σ/h in which σ is the surface tension [19]. Under these conditions, the yield stress fluid does not spontaneously spread, i.e., it resists gravity and/or capillary effects, and finally forms a deposit of significant thickness over the substrate, which differs from standard printed polymer-based materials. Another difference is that most pasty materials will in general only slowly further solidify (for example by drying or setting), which implies that the next layers may further deform the initial deposit. Finally, in the case of a yield stress fluid, the final shape of the deposit is not directly controlled by the nozzle cross section, it a priori depends a lot on the yield stress of the fluid. However, it is worth emphasizing that this yielding behavior can also be an advantage, as it allows to form, during the flow stage, specific, original deposit shapes, which the fluid will then essentially keep.

* Corresponding author.
E-mail address: philippe.coussot@univ-eiffel.fr (P. Coussot).

https://doi.org/10.1016/j.addma.2023.103752
Received 21 April 2023; Received in revised form 5 August 2023; Accepted 22 August 2023
Available online 25 August 2023

In practice, two main situations may be distinguished. Let us assume that the nozzle opening is cylindrical and imposes the initial filament diameter right after extrusion. If the distance between the nozzle and the substrate (plane) is smaller than the nozzle diameter the filament cannot simply curve while approximately keeping its diameter; as it is squeezed between the nozzle and the plane it has to somehow flow before reaching its deposited shape. Then, due to the yielding behavior of the fluid, the final thickness of the layer will remain close to the nozzle/plane distance. This situation is called layer (or lace) pressing [20]. It allows to have planar surfaces and thus a good adhesion between the successive layers. It moreover allows for a proper control of the overall geometrical accuracy of the printed element. One drawback is that pressing the layer induces an additional pressure to the whole structure, which can, in turn, lead to plastic collapse. If, on the contrary, the distance between the nozzle and the substrate is sufficiently large compared to the nozzle diameter, we expect a more limited deformation of the filament and, under some conditions, it is possible to get a deposit in the form of a continuous filament of thickness equal to the nozzle diameter.

In the present work we focus on the latter case, i.e., when the nozzle/plane distance is larger than the nozzle diameter, a situation which occurs in various contexts of additive manufacturing [3,5,6,21–25]. Here, we intend to present an overview of the deposit patterns that may be obtained depending on the material behavior and system characteristics, such as the extrusion velocity, the relative velocity between the plate and the nozzle, the distance between the nozzle and the substrate, and to find some general laws predicting the change of regimes.

Some aspects have already been studied, for example the formation then spreading of a deposit of a filament of yield stress fluid with significant capillary effects [26]. The conditions for buckling or tearing of a filament on the substrate [25,27], and possible instability in a corner [28], have been studied numerically. On another note, significant analytical and experimental developments were proposed for elastic materials [29,30] and Newtonian fluids [31–36], which surprisingly show that similar patterns of filament deposits (i.e., “discontinuous line”, “straight line”, “meanders”, “coils”) are obtained, despite the very different rheological behavior of these two material types. This similarity might in fact be of great importance for our analysis of yield stress fluid deposits, as it was demonstrated that, under some conditions, what essentially controls the patterns is the ratio of the length of deposited material over the surface to the length of relative displacement (nozzle/substrate) during a given time.

Note that the various fluids mentioned above are yield stress fluids possibly also exhibiting some viscoelasticity, thixotropy, aging or setting effects [1]. The characteristics of the deposit during a printing process will depend on the nozzle dimensions, the relative velocity between the nozzle and the ground, but also on these rheological characteristics. However, the most important rheological characteristics of these fluids in relation to the printing process is their yield stress, since this is the main origin of the flow stoppage and final shape of the filament.

Here we attempt to provide a generic framework of the shape of the deposit that may be obtained by extrusion from a nozzle in motion with respect to the substrate, as a function of dimensionless parameters involving the rheological characteristics of the fluid and the boundary conditions of the system. This will be done both from experimental data and theoretical considerations. In order to be able to focus on the impact of the yield stress only, thus avoiding perturbations due to other specific behavior characteristics, we use a model material exhibiting the behavior of a simple yield stress fluid, i.e., exhibiting negligible time-dependent properties such as viscoelasticity, thixotropy, aging or setting. Interestingly, we can prepare this model fluid at different solid fractions in a wide range, which allows to cover a large range of yield stress values with the same material type, which is hardly possible with any other material. This ensures the generality of our findings, which cover wide ranges of relative velocities, geometries and material behavior characteristics.

2. Material and methods

As a model yield stress fluid we used a kaolin suspension, i.e. a mixture of water and kaolin (clay). The kaolin particles are platelike with an equivalent spherical diameter of 2 μm. A homogeneous suspension is rapidly obtained by hand mixing the powder and water for a few minutes. The physical and rheological properties of this material were described in a previous works [37,38]. This material essentially exhibits a simple yield stress fluid behavior, i.e. with negligible viscoelastic effects, or thixotropy, aging or setting effects. The rheological behavior of the material is generally determined in simple shear, corresponding to the deformation or flow obtained when a sample layer is sheared by two parallel solid surfaces moving at a different velocity along the same direction parallel to the planes. In particular, one can thus determine the flow curve, i.e. the set of shear stress vs shear rate data in steady state flow, which reflects the flow characteristics in the liquid regime. In logarithmic scale such a flow curve exhibits a stress plateau at low shear rates corresponding to the material yield stress in simple shear (see Appendix 1): no steady state flow can be obtained below this value, the material behaves as a solid which can only undergo limited deformations. For the kaolin suspensions, still in logarithmic scale the flow curves approximately exhibit a similar shape at different concentrations (see [38]), i.e., they can superimpose if rescaled by the (yield) stress plateau value. As a consequence, we can characterize such a material with the help of its yield stress value, which increases with the solid fraction of the suspension. Here we will use suspensions with, from the smallest to highest concentration, a shear yield stress ranging from 150 to 1300 Pa, and a density ranging from 1390 to 1590 kg.m^{-3}.

It is worth noticing that for flows involved in printing processes, elongational deformations play a major role, either due to the compression of the extruded filament when the extrusion velocity is larger than the plane/nozzle velocity, or due to the extension and possibly breakage of the filament when the extrusion velocity is smaller than the plane/nozzle velocity. An elongational flow strongly differs from a simple shear flow: it typically corresponds to the uniform extension of a cylinder of material along its own axis. As a consequence, the rheological characteristics of the fluid which plays the major role in this context is the behavior of the material under simple elongational flows. Such a flow is more difficult to characterize, but we recently precisely developed an original approach for determining the steady state behavior of yield stress fluids under such conditions [37]. It appears that the corresponding flow curves for different yield stress values still superimpose if rescaled by the stress plateau at low strain rates, which is in fact the elongational yield stress, and this elongational yield stress is proportional to the simple shear yield stress [38]. It follows that either the elongational or the shear yield stress can be used as a reference rheological characteristics for these materials.

The printing system is a home-made device based on two indepen-

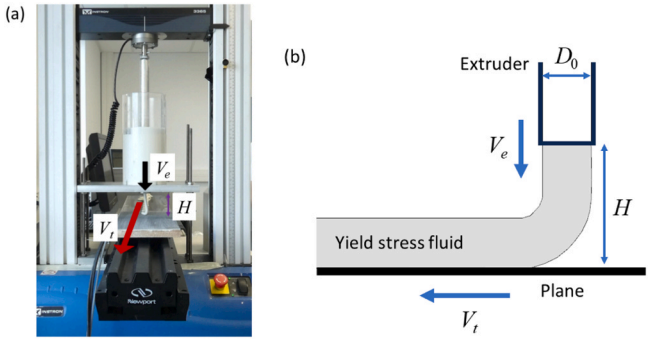

Fig. 1. (a) View of the set up allowing controlled relative displacement of the nozzle and the plane. (b) Scheme of principle of the extrusion of the yield stress fluid over a moving plane. Note that the real fluid shape depends on the relative values of the parameters, as explained in the text.

dent devices (see Fig. 1). The first one is an Instron 3600 traction-compression machine modified in such a way that the axis moves a piston inside a cylinder so as to push the paste through a nozzle of diameter D_0. D_0 was varied between 1.2 and 20 mm. The mean velocity of extrusion V_e, i.e. the flow rate divided by the nozzle cross-section area, is controlled by the piston velocity which is precisely imposed (to within 0.2%). The second device is a plane controlled by a linear motor and which can thus be translated over 80 cm at a (translation) velocity (V_t) ranging from 1 to 500 mm/s. The extrusion and plane translation are thus precisely controlled independently. Note that, since the flows are relatively slow, inertia effects are negligible, so that similar deposits are obtained whether the plane or the extrusion system is displaced, the only parameter being here the relative velocity between the nozzle and the plane.

Here we study only the first layer of material formed on the substrate. Note that the distance between the nozzle and the plane (i.e., H) was always larger than D_0, so that the flows are not in the layer pressing regime (see Introduction). Moreover, the deposit thickness being smaller than the filament diameter, is always smaller than 2 cm, while the yield stress is larger than 150 Pa, so that yield stress effects are significant with respect to gravity effects (τ_c is smaller or in the order of ρgh) and capillary effects (σ/D_0 is in the order or smaller than 60 Pa (using $\sigma = 0.07\mathrm{Nm}^{-1}$ [19])).

3. Experimental results

Let us consider a typical experiment with the kaolin paste with a given nozzle diameter and a fixed plate velocity. We look at the different phenomena occurring during the extrusion over the moving plate, for different velocities of extrusion and different heights (see Fig. 2). When the height is larger than a critical value the filament breaks before reaching the plate ($H = 7$cm in Fig. 2a). The drop size only slightly depends on the extrusion velocity up to a relatively large value of this velocity. For a smaller height, the filament reaches the plate before such breakage and thus forms elongated deposits ($H = 5$cm in Fig. 2a). Then it takes different shapes depending on the extrusion velocity. For small extrusion velocity, the filament, pulled by the plate in contact with it, breaks in pieces, thus forming a deposit shape which we call "discontinuous line" (see $V_e = 0.55\mathrm{cms}^{-1}$ in Fig. 2a). For somewhat higher velocity, it forms a uniform filament lying on the plate, a shape which we call "straight line" (see $V_e = 1\mathrm{cms}^{-1}$ in Fig. 2a). When the extrusion velocity is further increased the filament oscillates around its axis, a regime which we call "meandering" (see $V_e = 1.2\mathrm{cms}^{-1}$ in Fig. 2a) and finally for even higher velocity it forms loops, first "alternated loops" (see $V_e = 2\mathrm{cms}^{-1}$ in Fig. 2a) and then "translated loops" (see $V_e = 3.3\mathrm{cms}^{-1}$ in Fig. 2a). To illustrate the generality of these trends we carried a similar series of tests with a cement paste which is also a yield stress fluid but possibly with more complex addition properties (thixotropy). We can see in Fig. 2b that the different trends are very similar: filament breakage before reaching the plane for a sufficiently large height, then different filament shapes over the plane according to different ranges of the extrusion velocity.

We can now look more precisely at the distribution of these different patterns for the kaolin paste in a velocity vs height diagram when H and V_e vary over full ranges. Each pattern type is represented by a circle of a specific color. The different colors were chosen so as to provide clear and nice distinctions between the different regimes. We used the same colors for the same regimes all along the paper but, in some cases yellow dark was used instead of yellow for the sake of clarity. We obtain a diagram (see Fig. 3) in which different regions appear, associated with each of the basic patterns distinguished in Fig. 2a. In such a diagram the region of continuous deposit is approximately a rectangle situated below a critical velocity and a critical height. Inside this region we have a wide area in which straight lines are obtained, and three other areas which correspond to successive regions for increasing extrusion velocity, and in which we observe meandering, then alternated loops, then translated loops. Note that due to their strict definitions we can distinguish without ambiguity the regimes of discontinuous lines, alternated and translated loops, and the transition from discontinuous to straight lines. Concerning the transition from straight lines to meandering there might subsist some ambiguity as there could be some very slight meandering in the apparently straight lines. So, our definition of the straight line regime is here just the absence of visible meandering at our scale of observation (i.e., with eye). Curves associated with the frontier between the adjacent regions may be determined from such a diagram. They are built by joining all the points located at intermediate distance between two adjacent experimental points of two adjacent regions. Thus, we here assume these frontier curves follow the exact position of the transition of regimes as observed from our tests. However, due to the uncertainty on

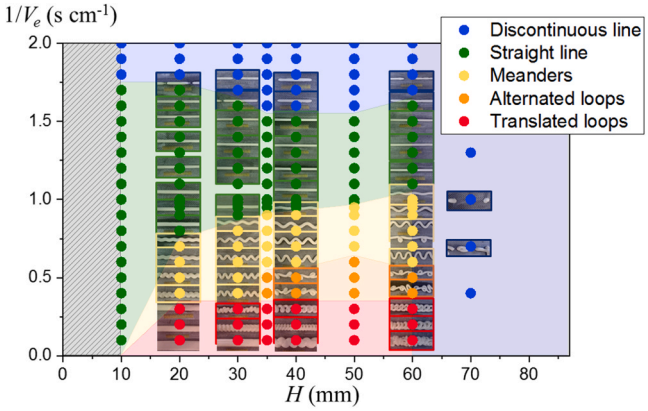

Fig. 3. Patterns of kaolin paste (300 Pa) deposits as a function of the height above plane and the extrusion velocity. The plane velocity is 1 cm.s^{-1} and the nozzle diameter 1 cm.

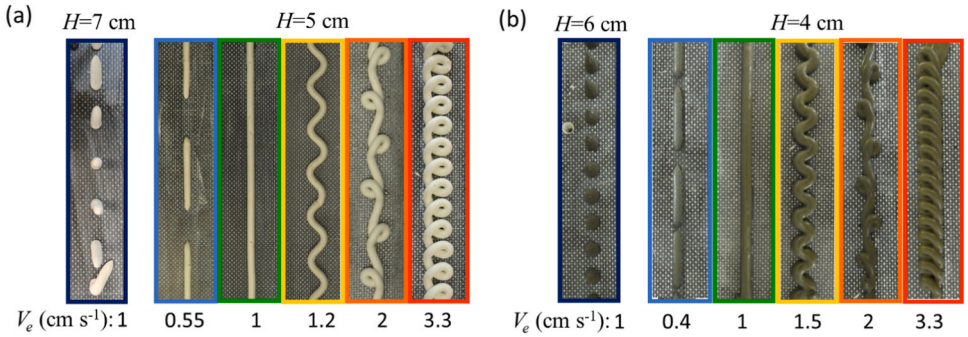

Fig. 2. : Basic patterns observed during the extrusion of a model yield stress fluid (a) (of yield stress 300 Pa) and a cement paste (b) of yield stress about 150 Pa, over a mobile plane, for different heights over the plane and different extrusion velocities. Here the nozzle diameter is 1 cm.

the material characteristics during the flow (some slight density heterogeneity may develop in the extrusion process of kaolin pastes [39]) and the details of the protocol (history of the upstream material flow), the frontier curves remain somewhat scattered. This scattering is illustrated from reproducibility tests (see Fig. 4) corresponding to three series of tests, each leading to a diagram of the type of Fig. 3, and carried out under the same conditions with the same material. Despite this scattering, the frontier curves appear to be robust, as they well superimpose and finally allow to clearly identify the different regions.

When varying the material properties, the plane velocity, the nozzle diameter, we obtain analogous diagrams, i.e., with qualitatively similar shapes of the different regions but with transitions associated with different critical velocities or heights. In the following we look in more details at the impact of these different parameters, which will provide key points for understanding the process.

3.1. Impact of the material yield stress

Changing the material behavior (here at different values of the shear yield stress in the range 150–1300 Pa induces a significant change of the results. A qualitatively similar diagram is obtained in each case: the same basic patterns and the same regions separated by frontier curves are obtained (see Fig. 5). However, the locations of these frontier curves significantly evolve as the yield stress increases. Looking more precisely at the data it appears that the difference essentially lies in the fact that, as the yield stress increases, the frontier curves look globally similar but they extend over a different height value before reaching the regions of droplets (see Fig. 6). In fact, they extend to a critical height H_c which increases with yield stress, and beyond which droplets are obtained.

Thus, at this stage, it may be suggested that: i) there exists a reference diagram for infinite yield stress, made of frontier curves extending over infinite height, and ii) each diagram of frontier curves for a finite yield stress value corresponds to the part for $H < H_c$ of this reference diagram, in which H_c depends on the yield stress, completed by a region of drop formation beyond H_c.

3.2. Impact of velocity

We have already seen a first impact of the velocity of extrusion for a fixed translation velocity: for$H < H_c$, when V_e increases we move from a discontinuous line to a continuous line region, and then to progressively more tortuous deposit shapes for larger V_e (see Figs. 3–5). For $H > H_c$ we observe drops for any V_e. This scheme is in fact valid below some critical extrusion velocity, typically in the order of 10 cm/s, and H_c does not

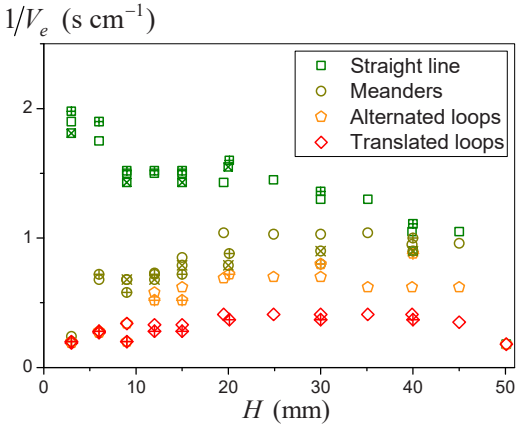

Fig. 4. Frontier curves for 3 series of tests with a kaolin paste (300 Pa) (empty, or different types of crossed symbols) carried out under similar conditions, as described in Fig. 3. The plane velocity is 1 cm.s^{-1} and the nozzle diameter 3 mm.

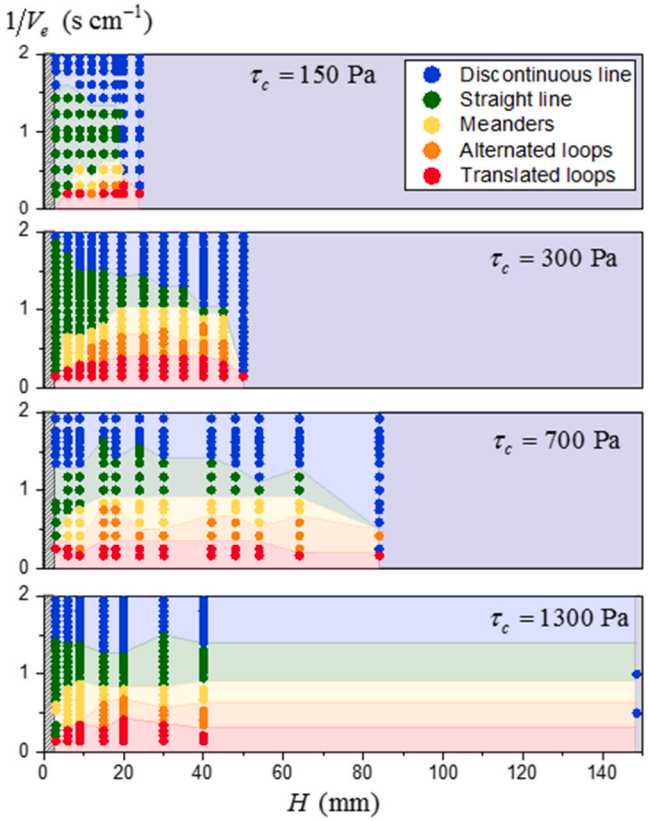

Fig. 5. : Diagram of patterns obtained during extrusion, over a moving plate (at 1 cm.s^{-1}) and with a nozzle diameter of 3 mm, of a kaolin paste at different yield stresses (see caption). Note that for the largest yield stress value (i.e., 1300 Pa) we only determined the critical height for breakage but did not carry out tests at heights intermediate between this value and 40 mm, so that the frontier curves were simply extended from the latter value along horizontal lines.

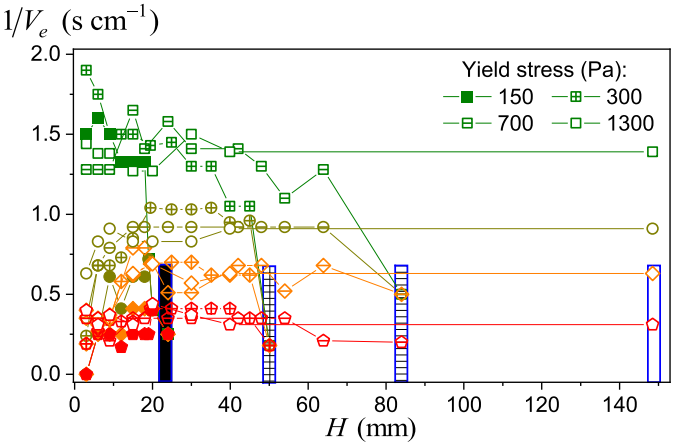

Fig. 6. : Frontier lines between the five different regions of the diagrams of Fig. 5. The same symbol filling type (either filled, crossed, lined, empty) corresponds to the same yield stress value (see legend), while the same symbol type and color correspond to the same frontier type: (from top to bottom) discontinuous lines to straight lines (green squares), straight lines to meandering (dark yellow circles), meandering to alternated loops (orange diamonds), alternated loops to translated loops (red hexagonal). The vertical blue rectangles, with the same filling type as for the corresponding yield stress, indicate the critical positions H_c associated with the different yield stress values.

vary significantly in this range. For a larger V_e the drops do not have enough time to form and separate before reaching the plane [38] so that a continuous though somewhat inhomogeneous line will form on the plane. We will not further consider this case in the present results and analysis, as it corresponds to rarely used velocity values in practice.

Finally, we can discuss more globally the impact of the translation velocity on the $(H, 1/V_e)$ diagram of patterns. In that aim we can compare the diagrams of deposit shapes obtained for $V_t = 1\text{cm.s}^{-1}$ and $V_t = 5\text{cm.s}^{-1}$. Qualitatively similar diagrams are obtained but with frontier curves situated at much lower $1/V_e$ values for $V_t = 5\text{cm.s}^{-1}$ than for $V_t = 1\text{cm.s}^{-1}$. This means that at larger translation velocities higher extrusion velocities are now necessary to get similar behavior. This suggests to consider the ratio of these two velocities as one of the main parameters of the process, $V^* = V_t/V_e$. Indeed, in a V^* vs H representation the two diagrams of the different deposit shape regions appear similar, i.e., the limiting curves are similar (see Fig. 7).

3.3. Impact of the nozzle diameter

We now vary the nozzle diameter in a wide range, i.e. between 1.2 and 20 mm. Once again we obtain the same qualitative diagrams exhibiting similar regions of basic patterns (see Fig. 8). However, in contrast with the case of yield stress variation, the region of continuous line does not vary much, it only slightly increases along the height axis, the critical height H_c increasing from 40 to 70 mm when D_0 is multiplied by about 17. An additional, more subtle, difference exists between these diagrams: the slope of the straight line frontier curve appears to decrease when D_0 increases (see Fig. 9a). This suggests that the height at which each slope of these curves is associated could increase with the characteristic length of the flow D_0. We can check further this assumption by plotting the data in a $V^*, H^* = H/D_0$ graph. Then the straight line frontier curves indeed appear to superimpose (see Fig. 9b). The same superimposition also appears for the meanders frontier curve. Remark that for the sake of clarity we did not represent the frontier curves for the two other regime transitions (i.e., towards alternated and translated loops) as the too large scattering on these curves does not allow to appreciate in details the validity of the superimposition assumption. Also note that in Fig. 9 the straight line and meanders frontier curves for $D_0 = 1.2\text{mm}$ does not superimpose well onto the curves for the other diameters, i.e., they are situated somewhat below the master curves (see Fig. 9b) but we have no clear explanation for that, since a potential discrepancy due to surface tension effects should also act on the first frontier curve (straight line). Finally, it must be emphasized that, in such a representation, the

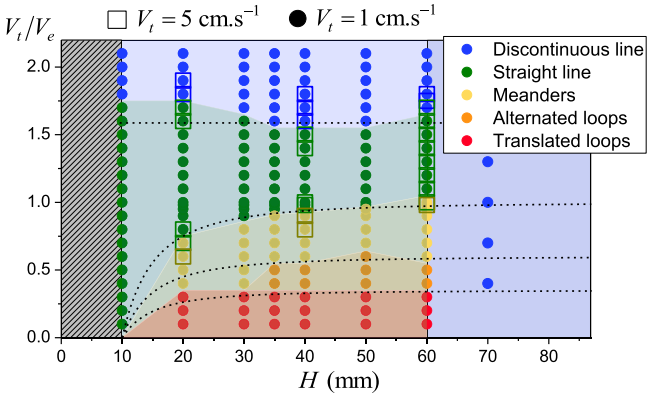

Fig. 7. Patterns of kaolin paste (300 Pa) deposits as a function of the height above plane and the ratio of the plane translation to the extrusion velocity, i.e., $V^* = V_t/V_e$. The nozzle diameter was 1 cm and the plane velocity was either 1 cm.s^{-1} (filled colored circles) or 5 cm.s^{-1} (open colored squares). The regions of transition between the different regimes are similar for both velocities. The dotted lines correspond to the theoretical frontier curves between the different regimes as suggested in the text (see Theoretical analysis).

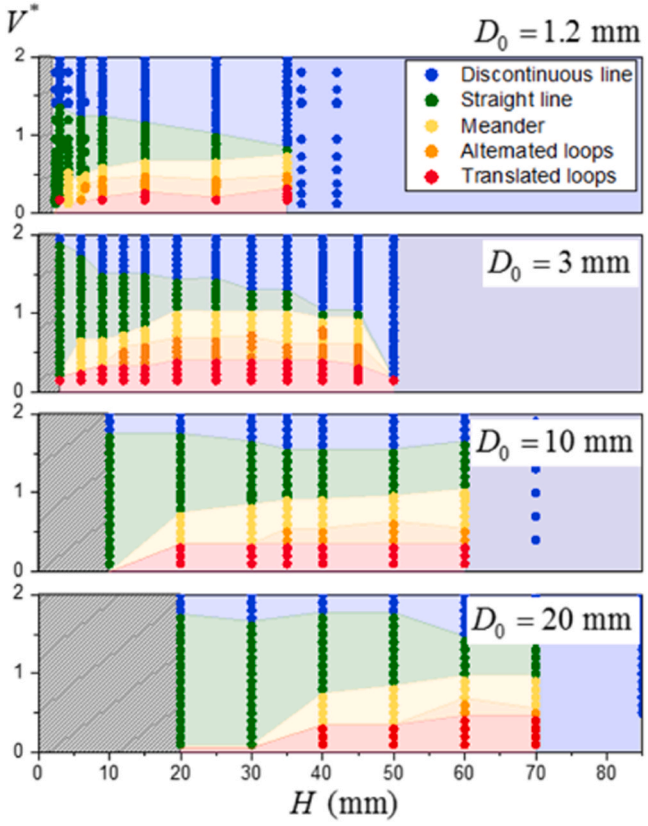

Fig. 8. Patterns of kaolin paste (300 Pa) deposits as a function of the height above plane and the ratio of the plane translation velocity and the extrusion velocity for different nozzle diameters. The plane velocity is 1 cm.s^{-1}.

critical height for the transition to drops now widely varies with D_0 (i.e. slightly faster than H_c/D_0)

The results above show that the yield stress has no particular impact on the observed patterns, it only impacts the filament shape when the latter has not yet reached the substrate. This means that gravity effects are negligible as soon as the filament has reached the substrate without breakage. Thus the patterns for the filament over the substrate are mainly governed by the geometry and the kinematics of the system. In the following, we will show that these different trends can be predicted from theoretical arguments.

4. Theoretical analysis

Our observations of clear trends for the patterns as a function of the extrusion velocity, the plane velocity, the nozzle height and diameter and the material yield stress, suggest that a rationalization, and even theoretical predictions, of these data, are possible.

In that aim we start by studying the trends observed for a large height. In that case the filament has time to elongate and finally break. This process has been the object of recent detailed studies [37,38]. The filament is deformed under the action of gravity: above the initially deformed region (see Fig. 10 a and c, region below A) the material elongates in each of its cross-sections as a result of the normal stress resulting from the weight of material situated below this section. Due to its yield stress fluid behavior, it is deformed up to a finite deformation as long as this normal stress is smaller than a critical value, i.e. the yield stress for elongation. In that case the material remains in its solid regime and it keeps a fixed shape as it further advances (see Fig. 10 b,c). When the yield stress is reached in some section (B in Fig. 10 c) the material starts to flow in its liquid regime, which means that the deformation is not limited any more. The flow is somewhat complex in this region,

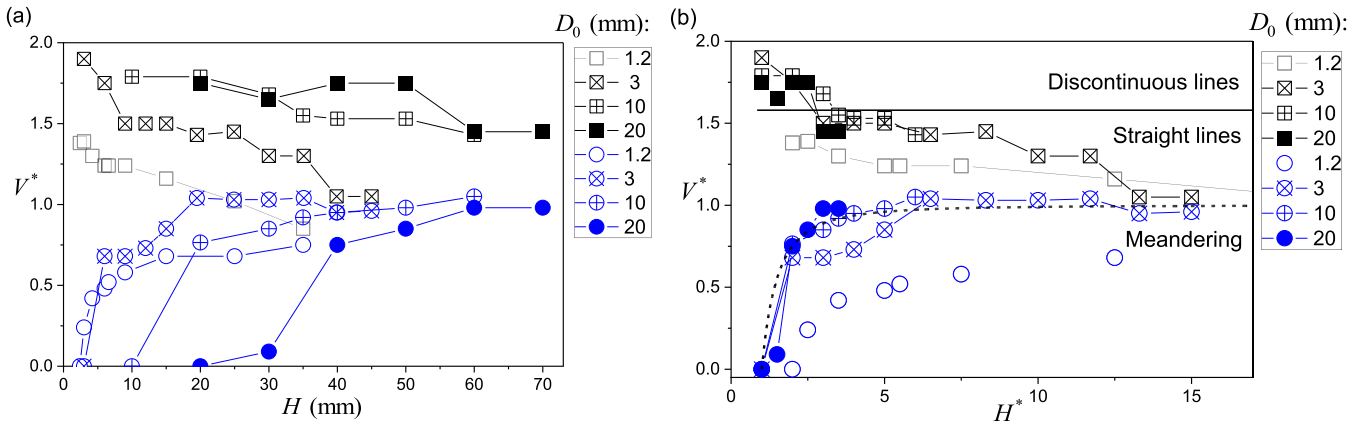

Fig. 9. Frontier curves between discontinuous and straight lines (squares) and between straight line and meandering (circles) as a function of the absolute height (a) or the height rescaled by nozzle diameter (b). Kaolin paste of yield stress 300 Pa, translation velocity 1 cm.s^{-1}. The lines correspond to the theoretical model (see text) for the transition between straight lines and meanders (dotted line), and for the transition between discontinuous lines and straight lines (continuous line).

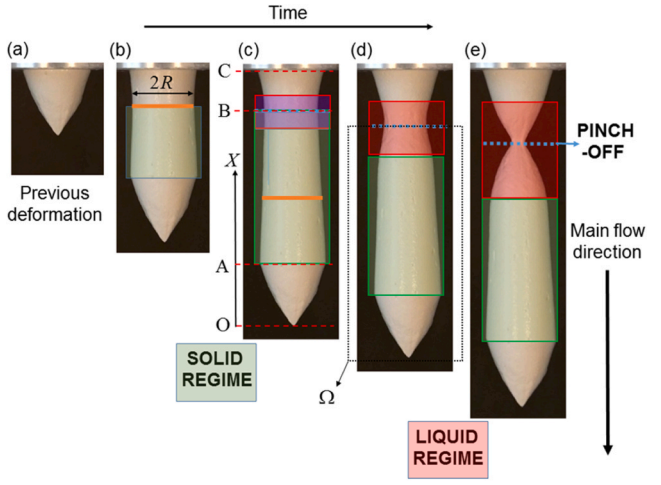

Fig. 10. Illustration of the different flow regimes during extrusion of a filament of yield stress fluid (here Kaolin, 27%, die diameter 2 cm) under gravity, just after the fall of the previous drop. Successive images of the filament: (a) Cone formed during previous drop fall, (b) and (c) Development of a region deformed in the solid regime, (d) and (e) Development of a region in the liquid regime and flow in this region. "Reproduced from [A. Geffrault, A., H. Bessaies-Bey, N. Roussel, P. Coussot, Instant yield stress measurement from falling drop size: the "syringe test", J. Rheology, 67 (2023) 305-314] with permission from the Society of Rheology (SOR)[38].

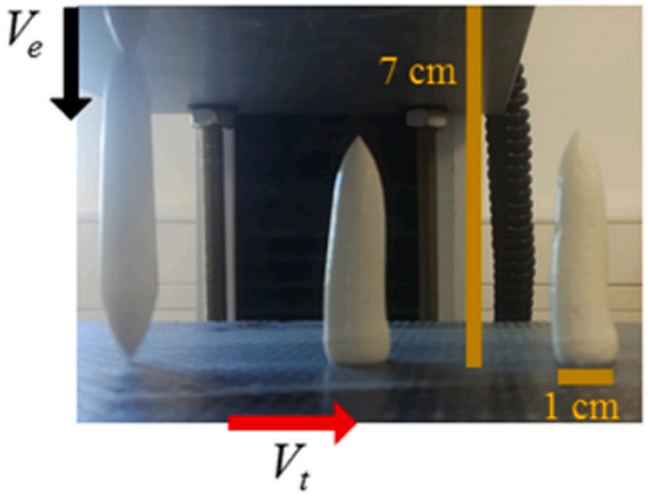

Fig. 11. Side view of the filament breakage as drops then forming mounds moving with the plane for $H > H_c$. $\tau_c = 300$Pa, and $V^* = 1$.

involving shear and extensional components, and implies that a region of finite height (see Fig. 10 d,e) is in the liquid regime and will undergo large deformations. Finally, the largest deformations are localized in the section where the yield stress was first reached, which leads to the pinch off of the filament followed by its breakage. Then we get the patterns shown in Fig. 11: the drops successively arrive on the plane and form a series of aligned mounds separated by a constant distance.

The above analysis may be used [38] to deduce the critical position of the pinch-off as a function of the elongational yield stress ($\sigma_{c,\text{elong.}}$).

$$\sigma_{c,\text{elong.}} = \frac{m_c g}{\pi {R_c}^2} \tag{1}$$

In which m_c is the droplet mass below pinch-off and R_c corresponds to the filament radius at the transition between the solid regime and the liquid regime, i.e., in the section B (see Fig. 10c). Its precise value depends on each material, but it appeared to be in the range 0.8 – 0.9 for different yield stress fluids [38]. This critical radius is associated with some critical strain at the solid-liquid transition, but based on existing knowledge it cannot be related to some straightforward comparison of the elastic behavior in the solid regime and the yield stress. Indeed, in general such materials also exhibit a plastic component in the solid regime, which increases as the stress approaches yielding [40].

The Eq. (1) may be used to deduce the length of the filament after breakage. First of all, we consider that the filament shape in the solid region, i.e., between A and B (see Fig. 10c), of length h_0, is conical. Secondly, we have to take into account, in the mass calculation, the previously deformed part (at the filament bottom) of approximately conical shape and of length about D_0, and the conical part resulting from the flow in the liquid region, here below the pinch-off. Assuming $R_0 - R_c$ is small compared to R_0 leads to $m_c \approx \rho\pi h_0 R_0 R_c + \rho\pi(4/3){R_0}^3$, and the effective length of the filament after breakage is equal to $h_0 + 2D_0$, since there are now two small conical regions at the bottom and the top of the drop. To get the total distance between the nozzle and the plane when the filament is just in contact with it, we have to add a conical region (below the nozzle) of height D_0, so that the critical height beyond which we should get drops is:

$$H_c \approx \frac{\sigma_c}{\rho g}\frac{R_c}{R_0} - \frac{4}{3}\frac{{R_0}^2}{R_c} + 6R_0 \tag{2}$$

Thus, our prediction is that the critical height beyond which we can get drops, i.e., filament breakage before it reaches the plane, is equal to

H_c. We can check the consistency of this prediction with our data, by comparing it with the experimental values for H_c as it can be estimated from the data of Figs. 6 and 8. We find a rather good agreement between the theoretical values (from Eq. (2)) and the experimental values (see Fig. 12). The theory appears to slightly overestimate the reality by, on average, about 12%.

Note that surface tension effects are negligible in our case since τ_c, larger than 150 Pa, and a fortiori $\sigma_{c,elong.}$ which is larger than τ_c [38], are much larger than σ/D_0, which is in the order of a few Pascals. Moreover, this conclusion remains valid during the filament breakage even in the pinch-off region, since the normal stress increases with $1/R^2$ while the surface tension stress increases more slowly, i.e., with $1/R$.

4.1. Filament evolution after contact with the plane

We now consider the case of a filament touching the ground before breakage, i.e., $H < H_c$. In that case the weight of material is mostly counterbalanced by the normal force from the plane, and thus plays a minor role on the filament deformation (a gravity stress significantly smaller than the yield stress inducing negligible deformations). Moreover, we assume a no-slip condition between the filament and the plane. This implies that, as soon as it touches the plane, the filament essentially moves, with a constant shape, at the speed of the plane. Under these conditions, as a first approximation we can see the filament deformation as mainly resulting from, at one side, the exit of a filament at a velocity V_e, and at the other side, its traction at a rate V_p in a direction perpendicular to the extrusion axis. Thus, from the regime of drop formation ($H > H_c$) to this regime ($H < H_c$) we turn from a controlled stress flow to a controlled strain flow.

In this context, for $V_e = V_p$, i.e., if $V^* = 1$, we expect to get a continuous filament with a diameter equal to that of the nozzle up to the plane, which is consistent with the mass conservation. If now V_e is smaller than V_p, i.e. for $V^* > 1$, we should get an elongation of the filament leading to a reduction of its radius (R) since now the plate tends to impose a faster motion than the extruder. Finally, for a sufficiently large value of V^*, when the deformation imposed to the filament is too large we expect a breakage of the filament (not induced by gravity effects). On the contrary, when V_e is larger than V_p, i.e. when $V^* < 1$, we expect some compression leading to an increase of the filament radius and possibly some instability leading to a large deformation of the filament axis.

These predictions indeed correspond to the different regions in our different experimental (V^*,H) diagrams presented above: discontinuous line beyond a critical value of V^*, continuous line for V^* around 1, and then compression and/or deformation of the filament below some critical V^* value depending on H.

Actually, the characteristics of the deformation of the material can be predicted theoretically in the case $V_e < V_t$. In that case, we can see the development of the process for V^* sufficiently close to 1 (here 1.5) (see Fig. 13a) and for a larger value (here 1.8) leading to filament breakage (see Fig. 13b). The flow rate imposed by the extrusion is $\pi {R_0}^2 V_e$, in which $R_0$is the filament radius at the extruder exit. As long as the filament deposit is straight (i.e., no instability) the flow rate imposed by the plane is equal to $\pi {R_p}^2 V_t$, in which $R_p$is the filament radius on the plane. The mass conservation imposes the equality of these flow rates, i.e., ${R_0}^2 V_e = {R_p}^2 V_t$. We deduce that, between the nozzle exit and the plane, the filament undergoes a total elongational deformation, i.e., $\varepsilon = \Delta R/R$, equal to $(R_0 - R_p)/R_0$, which thanks to the mass conservation may be rewritten as $\varepsilon = 1 - \sqrt{V_e/V_t}$. In fact, it seems that this deformation is rapidly reached after the nozzle exit (see Fig. 13), so that one can consider that as a first approximation the filament has a constant radius from the nozzle to the plane. Note that above, to estimate the elongational deformation, we neglected the curvature of the filament induced by the traction perpendicular to extrusion direction. This is justified by the fact that in this regime, beyond some short distance from the nozzle and the plane, the filament curvature remains small (see Fig. 13). This assumption (i.e., small curvature) is probably not valid any more when H becomes too small, since now the filament has to abruptly turn of 90° over a short distance, but it is difficult to evaluate the impact in terms of deformation and we will not elaborate further on this point.

In view of the above considerations concerning the filament breakage (under gravity) we expect to reach the liquid regime of the material when the deformation reaches a critical value ε_c, associated with the critical radius $R_c = (1 - \varepsilon_c)R_e$, and a plate velocity $V_t = (1 - \varepsilon_c)^{-2} V_e$, i.e., $V^* = (1 - \varepsilon_c)^{-2}$. Since the filament radius is obviously not perfectly uniform, the critical radius will be reached first at some point. Then, we soon get stronger deformations in this region since, in the liquid regime, the material can be widely deformed while the stress is close to the yield stress. Finally, the stress due to gravity becomes dominant and the filament falls onto the plane (see Fig. 13). For the kaolin pastes, according to previous observations of drop formation for simple flow under gravity [38] we can take $1 - \varepsilon_c \approx 0.8$ for all concentrations, which corresponds to $V_t/V_e \approx 1.56$. Beyond this value we reach the discontinuous line regime. Note that in practice we might have a slight deviation from this theoretical value which neglects the filament length associated with the flow in the liquid regime in the breakage region.

4.2. Buckling

We now consider the case of a rate of extrusion larger than the plane velocity, i.e., $V_e > V_t$ or $V^* < 1$. In that case, if the filament axis does not

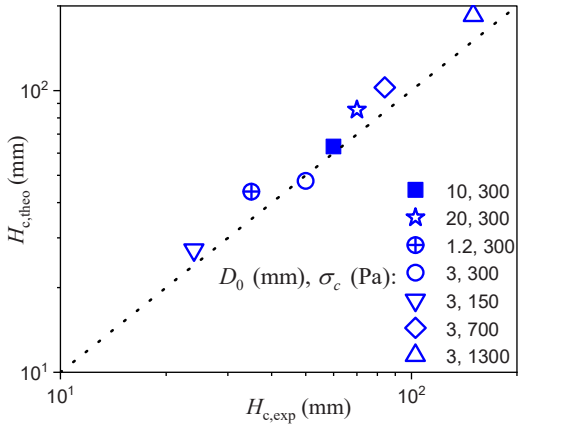

Fig. 12. : Theoretical prediction (see text) of the critical height ($H_{c,theo}$) for drop formation as a function of the observed critical height ($H_{c,exp}$) in our tests for different yield stress values and nozzle diameters.

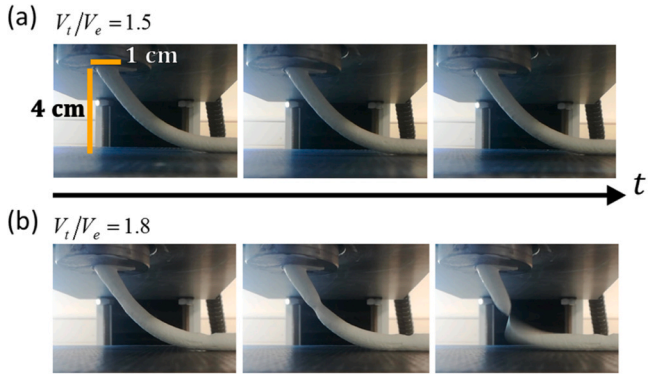

Fig. 13. Successive views (time frame of 0.06 s between two successive images) of the filament aspect in the straight line (a) and discontinuous line (b) regime. Yield stress: 300 Pa.

deviate from the plane motion direction, it will be compressed up to a radius $R_p = R_e\sqrt{V_e/V_t}$. However, the compression of a material with free lateral surfaces is a typical situation for which some instability can occur. This is buckling, which results in a deformation of the filament axis while its compression is smaller than that expected with compression only.

Buckling has been initially analyzed in depth in the case of elastic (solid) materials [41–43]. It was also later studied in the case of viscous fluids [44–46]. Here we are dealing with the flow of a yield stress fluid, for which, as far as we know, no theoretical approach predicting the conditions leading to buckling exists. However, we can remark that a similar criterion in terms of critical deformation for buckling was obtained for elastic and Newtonian materials [36]. Under these conditions, considering that by definition yield stress fluids exhibit rheological properties intermediate between an elastic solid and a simple viscous fluid, we suggest that the same criterion could be used. According to this criterion, obtained from scaling approaches [36], buckling will occur if the length of compression (ΔH) induced on the filament is larger than ${D_0}^2/L$, in which L is the length of the filament.

This criterion can be translated in terms of displacements of the filament. Let t_0 be the time needed for the filament to reach, as a result of extrusion, a length equal to the distance between the nozzle and the plane, i.e.,$L = H = V_e t_0$. During the same time ΔH is the difference of length resulting from the motion of the plane blocking the filament, i.e., $\Delta H = (V_e - V_t)t_0$, from which we deduce $\Delta H/H = 1 - V_t/V_e$. Our buckling criterion then writes:

$$V^* = 1 - \frac{\Delta H}{H} < 1 - \left(\frac{D_0}{H}\right)^2 = {V_c}^* \tag{3}$$

As soon as buckling occurs the filament will undergo very limited additional compression and it take different shapes depending on the relative values of the extrusion and plane velocities. Under these conditions, the filament behavior is essentially governed by the minimization of deformations in a given space, and thus these shapes can be expected to correspond to those observed and/or rationalized or predicted by numerical simulations in the case of simple viscous filaments [34,35,47]. Moreover, it was suggested that the patterns are robust with respect to a change in the thread rheology, i.e., *"the patterns can be described quantitatively by a non-linear ordinary differential equation which depends on three state variables only, and is geometric in essence."* [35], which supports the use of these limits for a yield stress fluid.

Here we suggest to use the mean values obtained by these authors [35,48] under different conditions of transitions (which we could not distinguish in our case), which gives approximately 0.35 and 0.6, respectively for the transition from meandering to alternated loops and then to translated loops. As a consequence, for slender filament we expect simple meandering as long as $0.6 < V^* < 1$, alternated loops for $0.35 < V^* < 0.6$ and translated loops for $V^* < 0.35$. However, for these works concerning other material types no compression and slender filaments were assumed, which in particular led to consider this transition from straight lines to meandering for ${V_c}^* = 1$. In fact, when H approaches D_0 we do not have slender filaments, and we can hardly expect another shape than that obtained by simple compression, thus no other regime can occur, which can be expressed by considering that the above limits between the different regimes fall down to $V^* = 0$ when $H = D_0$. On the other side we would recover the above limits for slender filament for $H >> D_0$. These trends are in particular consistent with the variations of ${V_c}^*$ as expressed in Eq. (3). Here, our assumption is that we have variations of the other limits similar to those of ${V_c}^*$, i.e. the limit between meandering and alternated loops is $0.6{V_c}^*$ and the limit between alternated loops and translated loops is $0.35{V_c}^*$.

To sum up, the different patterns obtained in such a process can be predicted theoretically in a general way according to the following criteria:

1) Droplets resulting from flow under gravity for $H > H_c$
2) Discontinuous lines due to filament breakage for $V^* > (1-\varepsilon_c)^{-2}$
3) Continuous line for $1 - (D_0/H)^2 = {V_c}^* < V^* < (1-\varepsilon_c)^{-2}$
4) Meandering for $0.6{V_c}^* < V^* < {V_c}^*$
5) Alternated loops for $0.35{V_c}^* < V^* < 0.6{V_c}^*$
6) Translated loops for $V^* < 0.35{V_c}^*$

This gives the universal mapping of the patterns as represented in Fig. 14.

We can now review the results to appreciate the agreement of this general theoretical diagram with the reality. The frontier curve between discontinuous line and straight line indeed approximately corresponds to a horizontal line in any case, as described here by the theory, i.e., depending only on the critical deformation of the material type, as may be seen from its constant level around $V^* = 1.5$ whatever the system characteristics and material yield stress (see e.g., Figs. 6, 7, 9). The frontier curve for the transition to drops is indeed a vertical line (see Fig. 7) located at a critical value for H which essentially depends on the material yield stress but also on the filament diameter, according to Eq. (2) (see Fig. 12). Finally, the data well superimpose when represented in a diagram V^* vs H^* for a fixed yield stress value (see Figs. 7, 9) and the frontier curves are in excellent agreement with the theoretical ones indicated above (see e.g., Figs. 7 and 9).

Note that along all the above considerations we implicitly assumed that only the geometrical characteristics including the velocity ratio, and the yield stress through the critical height for breakage, govern the deposit shape characteristics. Actually, the typical behavior of a yield stress fluid beyond the yield stress, i.e., in the liquid regime, is described by a constitutive equation in which the stress is the sum of a constant term (the yield stress) and a term depending on the shear rate [1], which is in fact the local gradient of velocity. The most frequently used model is the Herschel-Bulkley model (see Appendix 1), which allows to represent the simple shear behavior in a wide range of shear rates [1]. As long as the second term of the model is negligible compared to the yield stress the stress is approximately equal to the yield stress so that the response of the material to deformations essentially involves stress values close to the yield stress. For a material whose behavior is represented by a Herschel-Bulkley model, the ratio of the velocity dependent term to the yield stress may be estimated through the Bingham number $Bi = \tau_c/k(\dot{\gamma}_0)^n$, in which $\dot{\gamma}_0$ is a characteristic shear rate of the flow. A similar expression with now the elongational yield stress and a characteristic elongational rate may be used if extensional flow is dominant. However, for our experiments, considering the diversity and complexity of flow characteristics in the different regions of the filament and in the

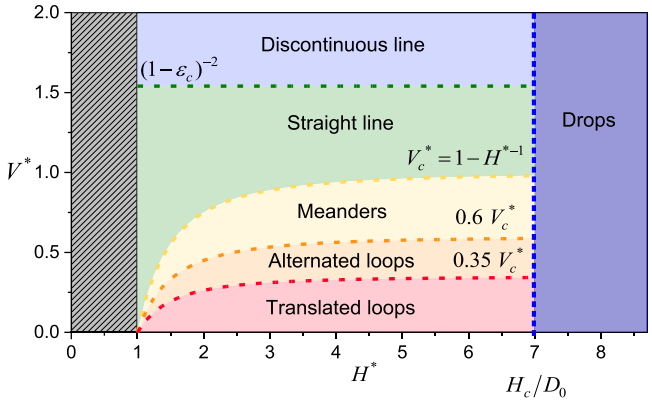

Fig. 14. Universal mapping of patterns obtained by extrusion of a yield stress fluid filament over a moving plane, as a function of the velocity ratio and the height rescaled by the nozzle diameter. The frontier curves are represented as dotted lines, associated with the mentioned equations (using here $1 - \varepsilon_c = 0.8$). Note that the position of the frontier curve for drop formation depends on the yield stress value through the value ofH_c.

different regimes, it does not appear possible to provide complete precise estimations of the characteristic shear or elongational rate. An additional complication is that this approach is valid only in the liquid regime of the material, and we cannot really determine the flow regime at the different steps of the flow but it is likely that the fluid remains in its solid regime during a significant fraction of the flow until it finally fully stops over the plane and remains rigid. This complexity justifies that we rely on the consistency of our data with regards to the variation of the different parameters and the analysis in geometrical terms, along with the absence of impact of the velocity ratio in our range of tests, to conclude that the yield stress is the only rheological parameter playing a role in this context.

5. Conclusion

This work shows that it is possible to predict the different patterns which can be obtained during the printing of yield stress fluids on the basis of a minimal knowledge of the system. A mapping of these patterns may then be drawn as a function of the ratio of plane velocity to extrusion rate and the height rescaled by the nozzle diameter. Two frontier curves depend on the rheological characteristics of the fluid, more precisely its critical deformation and yield stress associated with the transition from the solid to the liquid behaviour in elongation. These parameters may be estimated from independent tests of filament breaking in drops under gravity [34]. Here we considered a simple yield stress fluid, but we can expect these results to well apply as a first approximation to more complex materials exhibiting some elasticity, aging or thixotropy, as long as the yielding effect is dominant.

Ethics approval and consent to participate

Not applicable.

Consent for publication

Not applicable.

Competing interests

The authors declare that they have no competing interests.

Funding

A.G. work was supported by a grant from Université Gustave Eiffel.

CRediT authorship contribution statement

Anatole Geffrault: Writing – original draft, Visualization, Validation, Methodology, Investigation, Data curation, Conceptualization. **Hela Bessaies-Bey:** Writing – review & editing, Supervision, Resources, Methodology, Formal analysis. **Philippe Coussot:** Writing – review & editing, Writing – original draft, Validation, Resources, Project administration, Methodology, Formal analysis, Conceptualization, Supervision**. Nicolas Roussel:** Writing – review & editing, Supervision, Project administration, Methodology, Formal analysis, Conceptualization**.** All authors reviewed the manuscript.

Declaration of Competing Interest

The authors declare that they have no known competing financial interests or personal relationships that could have appeared to influence the work reported in this paper.

Data Availability

Data will be made available on request.

Acknowledgements

We are grateful to P.-T. Brun for a very enlightening discussion on this subject.

Appendix 1. Flow curve of a kaolin paste

Fig. 15 shows the typical behavior of a kaolin paste, as it is obtained from simple shear rheometrical tests. Here a decreasing shear stress is progressively applied (in a parallel disks geometry [34]) and the corresponding shear rate (velocity gradient) at each level is recorded.

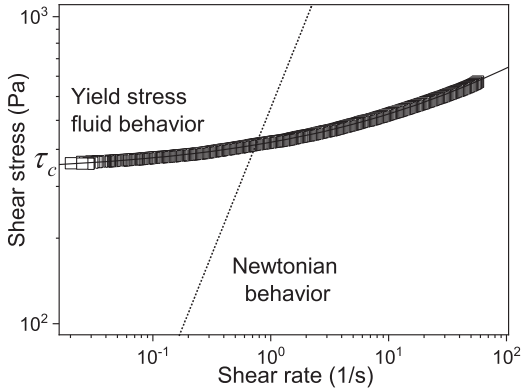

Fig. 15. Flow curve of a kaolin paste. The dotted line shows the flow curve of a Newtonian fluid. The continuous line is a Herschel-Bulkley model ($\tau > \tau_c \Rightarrow \tau = \tau_c + k\dot{\gamma}^n$, in which $\dot{\gamma}$ is the shear rate and k and n are two material parameters) fitted to these data with $\tau_c = 310\text{Pa} k = 80\text{Pa.s}^{-n}$ and $n = 1/3$.

.

References

[1] P. Coussot, Rheometry of pastes, suspensions and granular materials, Wiley, New York, 2005.

[2] F. Bos, R. Wolfs, Z. Ahmed, T. Salet, Additive manufacturing of concrete in construction: potentials and challenges of 3D concrete printing, Virtual Phys. Prototyp. 11 (2016) 209–225, https://doi.org/10.1080/17452759.2016.1209867.

[3] H. Jeong, S.-J. Han, S.-H. Choi, Y.J. Lee, S.T. Yi, K.S. Kim, Rheological property criteria for buildable 3D printing concrete, Materials 12 (2019) 657–677, https://doi.org/10.3390/ma12040657.

[4] V. Mechtcherine, F.P. Bos, A. Perrot, W.R. Leal da Silva, V.N. Nerella, S. Fataei, R.J. M. Wolfs, M. Sonebi, N. Roussel, Extrusion-based additive manufacturing with cement-based materials - PRODuction steps, processes, and their underlying physics: a review, Cem. Concr. Res. 132 (2020), 106037, https://doi.org/10.1016/j.cemconres.2020.106037.

[5] A. Perrot, D. Rangeard, E. Courteille, 3D printing of earth-based materials: processing aspects, Constr. Build. Mater. 172 (2018) 670–676, https://doi.org/10.1016/j.conbuildmat.2018.04.017.

[6] A. Perrot, D. Rangeard, A. Pierre, Structural built-up of cement-based materials used for 3Dprinting extrusion techniques, Mater. Struct. 49 (2016) 1213–1220, https://doi.org/10.1617/s11527-015-0571-0.

[7] Roussel, Rheological requirements for printable concretes, Cem. Concr. Res. 112 (2018) 76–85, https://doi.org/10.1016/j.cemconres.2018.04.005.

[8] U. Daalkhaijav, O.D. Yirmibesoglu, S. Walker, Y. Menguc, Rheological modification of liquid metal for additive manufacturing of stretchable electronics, Adv. Mater. Technol. 3 (2018) 1700351, https://doi.org/10.1002/admt.201700351.

[9] S. Tagliaferri, A. Panagiotopoulos, C.J.M.A. Mattevi, Direct ink writing of energy materials, Mater. Adv. 2 (2021) 540–563, https://doi.org/10.1039/D0MA00753F.

[10] A. M'Barki, L. Bocquet, A. Stevenson, Linking rheology and printability for dense and strong ceramics by direct ink writing, Sci. Rep. 7 (2017) 1–10, https://doi.org/10.1038/s41598-017-06115-0.

[11] S. Zhu, M.A. Stieger, A.J. Van der Goot, M.A.I. Schutyser, Extrusion-based 3D printing of food pastes: correlating rheological properties with printing behavior, Innov. Food Sci. Emerg 58 (2019), 102214 https://doi.org/10.1016/j.ifset.2019.102214.

[12] R. Karyappa, M. Hashimoto, Chocolate-based ink three-dimensional printing (Ci3DP), Sci. Rep. 9 (2019) 14178, https://doi.org/10.1038/s41598-019-50583-5.

[13] J.M. Townsend, E.C. Beck, S.H. Gehrke, C.J. Berkland, M.S. Detamore, Flow behavior prior to crosslinking: the need for precursor rheology for placement of hydrogels in medical applications and for 3D bioprinting, Prog. Polym. Sci. 91 (2019) 126–140, https://doi.org/10.1016/j.progpolymsci.2019.01.003.

[14] A.Z. Nelson, B. Kundukad, W.K. Wong, S.A. Khan, P.S. Doyle, Embedded droplet printing in yield-stress fluids, PNAS 117 (2020) 5671–5679, https://doi.org/10.1073/pnas.1919363117.

[15] B. Wu, K.D. Song, D.M. Zhang, B. Ren, M. Sole-Gras, Y. Huang, J. Yin, Embedded extrusion printing in yield-stress-fluid baths, Matter 5 (2022) 3775–3806, https://doi.org/10.1016/j.matt.2022.09.003.

[16] L.M. Friedrich, J.E. Seppala, Simulated filament shapes in embedded 3D printing, Soft Matter 17 (2021) 8027–8046, https://doi.org/10.1039/d1sm00731a.

[17] Q. Wu, F.B. Zhu, Z.L. Wu, Y. Xie, J. Qian, J. Yin, H.Y. Yang, Suspension printing of liquid metal in yield-stress fluid for resilient 3D constructs with electromagnetic functions, npj Flexible, Electronics 6 (2022) 50, https://doi.org/10.1038/541528-022-00184-6.

[18] P. Coussot, S. Proust, C. Ancey, Rheological interpretation of deposits of yield stress fluids, J. Non-Newton. Fluid Mech. 66 (1996) 55–70, https://doi.org/10.1016/0377-0257(96)01474-7.

[19] J. Boujlel, P. Coussot, Measuring the surface tension of yield stress fluids, Soft Matter 9 (2013) 5898–5908, https://doi.org/10.1039/C3SM50551K.

[20] P. Carneau, R. Mesnil, O. Baverel, N. Roussel, Layer pressing in concrete extrusion-based 3D-printing: Experiments and analysis, Cem. Concr. Res. 155 (2022), 106741, https://doi.org/10.1016/j.cemconres.2022.106741.

[21] B. Khoshnevis, Automated construction by contour crafting - related robotics and information technologies, Autom. Constr. 13 (2004) 5–19, https://doi.org/10.1016/j.autcon.2003.08.012.

[22] R.A. Buswell, W.R.L. da Silva, F.P. Bos, H.R. Schipper, D. Lowke, N. Hack, H. Kloft, V. Mechtcherine, T. Wangler, N. Roussel, A process classification framework for defining and describing Digital Fabrication with Concrete, Cem. Concr. Res. 134 (2020), 106068, https://doi.org/10.1016/j.cemconres.2020.106068.

[23] T. Wangler, E. Lloret, L. Reiter, N. Hack, F. Gramazio, M. Kohler, M. Bernhard, B. Dillenburger, J. Buchli, N. Roussel, R. Flatt, Digital Concrete: opportunities and challenges, RILEM Tech. Lett. 1 (2016) 67–75, https://doi.org/10.21809/rilemtechlett.2016.16.

[24] R.J.M. Wolfs, F.P. Bos, T.A.M. Salet, Early age mechanical behaviour of 3D printed concrete: numerical modelling and experimental testing, Cem. Concr. Res. 106 (2018) 103–116, https://doi.org/10.1016/j.cemconres.2018.02.001.

[25] A.S.J. Suiker, R.J.M. Wolfs, S.M. Lucas, T.A.M. Salet, Elastic buckling and plastic collapse during 3D concrete printing, Cem. Concr. Res. 135 (2020), 106016, https://doi.org/10.1016/j.cemconres.2020.106016.

[26] J. Van der Kolk, D. Tieman, M. Jalaal, Viscoplastic lines: printing a single filament of yield stress material on a surface, J. Fluid Mech. 958 (2023) A34, https://doi.org/10.1017/jfm.2023.118.

[27] R.J.M. Wolfs, T.A.M. Salet, N. Roussel, Filament geometry control in extrusion-based additive manufacturing of concrete: The good, the bad and the ugly, Cem. Concr. Res. 150 (2021), 106615, https://doi.org/10.1016/j.cemconres.2021.106615.

[28] R. Comminal, M.P. Serdeczny, D.B. Pedersen, J. Spangenberg, Motion planning and numerical simulation of material deposition at corners in extrusion additive manufacturing, Addit. Manuf. 29 (2019), 100753, https://doi.org/10.1016/j.addma.2019.06.005.

[29] M. Habibi, N.M. Ribe, D. Bonn, Coiling of elastic ropes, Phys. Rev. Lett. 99 (2007), 154302, https://doi.org/10.1103/PhysRevLett.99.154302.

[30] M. Habibi, J. Najafi, N.M. Ribe, Pattern formation in a thread falling onto a moving belt: an "elastic sewing machine", Phys. Rev. E 84 (2011), 016219 https://doi.org/10.1103/PhysRevE.84.016219.

[31] S. Chiu-Webster, J.R. Lister, The fall of a viscous thread onto a moving surface: a 'fluid-mechanical sewing machine', J. Fluid Mech. 569 (2006) 89–111, https://doi.org/10.1017/S0022112006002503.

[32] S.W. Morris, J.H.P. Dawes, N.M. Ribe, J.R. Lister, Meandering instability of a viscous thread, Phys. Rev. E 77 (2008), 066218, https://doi.org/10.1103/PhysRevE.77.066218.

[33] M. Habibi, Y. Rahmani, N.M. Daniel Bonn, Ribe, Buckling of liquid columns, Phys. Rev. Lett. 104 (2010), 074301, https://doi.org/10.1103/PhysRevLett.104.074301.

[34] P.-T. Brun, N.M. Ribe, y, A numerical investigation of the fluid mechanical sewing machine, Phys. Fluids 24 (2012), 043102, https://doi.org/10.1063/1.3703316.

[35] P.-T. Brun, B. Audoly, N.M. Ribe, T.S. Eaves, J.R. Lister, Liquid ropes: a geometrical model for thin viscous jet instabilities, Phys. Rev. Lett. 114 (2015), 174501, https://doi.org/10.1103/PhysRevLett.114.174501.

[36] M. Le Merrer, D. Quéré, C. Clanet, Buckling of viscous filaments of a fluid under compression stresses, Phys. Rev. Lett. 109 (2012), 064502, https://doi.org/10.1103/PhysRevLett.109.064502.

[37] A. Geffrault, H. Bessaies-Bey, N. Roussel, P. Coussot, Extensional gravity-rheometry (EGR) for yield stress fluids, J. Rheol. 65 (2021) 887–901, https://doi.org/10.1122/8.0000241.

[38] A. Geffrault, A., H. Bessaies-Bey, N. Roussel, P. Coussot, Instant yield stress measurement from falling drop size: the "syringe test", J. Rheol. 67 (2023) 305–314, https://doi.org/10.1122/8.0000557.

[39] B.D. Rabideau, P. Moucheront, F. Bertrand, S. Rodts, Y. Melinge, C. Lanos, P. Coussot, Internal flow characteristics of a plastic kaolin suspension during extrusion, J. Am. Ceram. Soc. 95 (2012) 494–501, https://doi.org/10.1111/j.1551-2916.2011.04882.x.

[40] E. Ngouamba, P. Coussot, Elastoplastic behavior of yield stress fluids, Phys. Rev. Fluids 4 (2019), 123301, https://doi.org/10.1103/PhysRevFluids.4.123301.

[41] L. Euler, Methodus inveniendi lineas curvas maximi minimive proprietate gaudentes, sive, Solutio problematis isoperimetrici latissimo sensu accepti. Genevæ: Apud Marcum-Michaelem Bousquet & Socios, (1744) https://doi.org/10.5479/sil.318525.39088000877480.

[42] A. Love, A. Treatise on the Mathematical Theory of Elasticity on the Mathematical Theory of Elasticity, Cambridge University Press, Cambridge, 1927.

[43] E.H. Dill, Kirchhoff's theory of rods, Archive for History of Exact, Sciences 44 (1992) 1–23.

[44] V.M. Entov, A.L. Yarin, The dynamics of thin liquid jets in air, J. Fluid Mech. 140 (1984) 91–111, https://doi.org/10.1017/S0022112084000525.

[45] G.I. Taylor, Instability of jets, threads, and sheets of viscous fluid, Appl. Mech. (1969) 382–388, https://doi.org/10.1007/978-3-642-85640-2_30.

[46] B. Tchavdarov, A.L. Yarin, et S. Radev, Buckling of thin liquid jets, J. Fluid Mech. 253 (1993) 593–615, https://doi.org/10.1017/S0022112093001910.

[47] H. Yuk, X. Zhao, A new 3D printing strategy by harnessing deformation, instability, and fracture of viscoelastic inks, Adv. Mater. 30 (6) (2018) 1704028, https://doi.org/10.1002/adma.201704028.

[48] N.M. Ribe, P.-T. Brun, B. Audoly, Symmetry and asymmetry in the fluid mechanical sewing machine, Symmetry 14 (2022) 772, https://doi.org/10.3390/sym14040772.